PAPER

Check for updates

Magnetic properties of coordination clusters with {Mn₄} and {Co₄} antiferromagnetic cores†

Simona Achilli, [iD] *[ab] Claire Besson, [iD] [c] Xu He, [iD] [d] Pablo Ordejón, [iD] [d]
Carola Meyer [iD] [e] and Zeila Zanolli [iD] [bdf]

We present a joint experimental and theoretical characterization of the magnetic properties of coordination clusters with an antiferromagnetic core of four magnetic ions. Two different compounds are analyzed, with Co and Mn ions in the core. While both molecules are antiferromagnetic, they display different sensitivities to external magnetic field, according to the different atomic magnetic moments and strength of the intra-molecular magnetic couplings. In particular, the dependence of the magnetization *versus* field of the two molecules switches with temperature: at low temperature the magnetization is smaller in {Mn₄} than in Co₄, while the opposite happens at high temperature. Through a detailed analysis of the electronic and magnetic properties of the two compounds we identify a stronger magnetic interaction between the magnetic ions in {Mn₄} with respect to {Co₄}. Moreover {Co₄} displays not negligible spin–orbit related effects that could affect the spin lifetime in future antiferromagnetic spintronic applications. We highlight the necessity to account for these spin–orbit effects together with electronic correlation effects for a reliable description of these compounds.

1 Introduction

Molecular magnets constitute an excellent platform for molecular spintronics and quantum information storage and processing as their properties can be controlled at the nano/micro-scale during fabrication.[1–3] Coordination clusters formed by an inner magnetic core and a surrounding shell of organic ligands can be synthesized to control both the magnetic interactions between the ions within the molecule and the coupling between magnetic core and environment,[4] while practically reducing to nothing the influence of inter-molecular interactions on the magnetic properties. Single-molecule magnets are particularly attractive for spin-dependent quantum transport applications[5] as the spin retains its orientation in the absence of an external magnetic field and

applications can leverage on the technology developed for functionalization with nanoparticles.[6,7]

In recent years, research has concentrated on molecular magnets with large overall spin generated by ferromagnetic coupling between magnetic centers.[8–10] On the other hand, the incorporation of molecular antiferromagnets in spintronic devices[11,12] is still a new area of research. Recent proposals are only theoretical, and concern molecular AFM crystals[13] or systems that can hardly be realized experimentally.[14] The expected advantages of antiferromagnetic coordination clusters are the same as for antiferromagnetic spintronic devices, *i.e.* robustness against perturbation due to magnetic fields, absence of stray fields, and capability to generate ultrafast dynamics and large magnetotransport effects.[15] Antiferromagnetic molecules can be used to functionalize other organic systems, as carbon nanotubes, with the advantage that the current flowing through the tube does not alter the magnetic properties of the molecules[16,17] and the low spin–orbit coupling allows long spin-flip lengths and spin lifetimes.

The application of molecular magnets in spintronics and quantum technologies would benefit from molecular design aimed at identifying the most suitable combinations of magnetic ions and organic ligands to ensure long spin coherence times, efficient spin injections and tunable transitions between spin states.[18–20] Property-tuning efforts are usually concentrated on modifications of the ligands surrounding a given metal core. This approach, however, has some limitations for integrating the molecule in a device: the ligands are also the place where the

ª Dipartimento di Fisica "Aldo Pontremoli", Universitá degli Studi di Milano, Via Celoria 16, Milan, Italy. E-mail: simona.achilli@unimi.it

ᵇ European Theoretical Spectroscopy Facilities

ᶜ Department of Chemistry, The George Washington University, Washington, D'C 20052, USA

ᵈ Catalan Institute of Nanoscience and Nanotechnology - ICN2 (CSIC and BIST), Campus UAB, Bellaterra, 08193 Barcelona, Spain

ᵉ Department of Physics, Universität Osnabrück, 49076 Osnabrück, Germany

ᶠ Chemistry Department, Debye Institute for Nanomaterials Science, Condensed Matter and Interfaces, Utrecht University, PO Box 80 000, 3508 TA Utrecht, The Netherlands

† Electronic supplementary information (ESI) available: Full experimental details, Heisenberg fit of the SQUID data. Spin dynamics calculation. Relaxed structures. See DOI: 10.1039/d1cp03904k

interaction with the environment takes place. Changing the ligands can have unwanted and unpredictable effects on the electronic properties of the device-molecule interface, in addition to changes of the magnetic properties of the core. We propose here a reverse approach: the ligand system is kept identical, and the magnetic properties are modified by changing the metal atoms.

We selected the architecture of a M_4O_4 cubane structure based on the family of {Mn_4} antiferromagnets with the general formula $[(RCO_2)_4Mn_4L_2]$ (R = CF$_3$, CH$_3$, Ph, H$_2$L = 2,6-bis(1-(2-hydroxyphenyl)iminoethyl)pyridine) previously reported by Kampert *et al.*[21] The presence of four metal centers offers a rich landscape of electronic and magnetic levels for spintronic applications. Through a joint experimental and theoretical characterization we compare the {Mn_4} acetate complex with its newly prepared cobalt analogue.

Many M_4O_4 cubane complexes are reported in the literature, for M = Co and Mn. However, their magnetic properties have been investigated only in four cases[22–25] showing a switching or an enhancement of the magnetic coupling by changing the inner core. In $[M_4(dpd-H)_4(OAc)_3(OH_2)_1]^+$ and $[M_4(dpd-H)_4(OAc)_2\{N(CN)_2\}_2]$ (dpd-H$_2$ = di-2-pyridylketone in gem-diol form), the overall magnetic coupling shifts from antiferromagnetic for manganese(II) centers to ferromagnetic for cobalt(II).[22,23] In $[M_4(cit)_4]^{8-}$ (cit = citrate) and $[M_4(nic)_4(OMe)_4]$ (nic = nicotinate) the coupling is antiferromagnetic for both ions, but the coupling is larger for manganese in the former case[24] and for cobalt in the latter.[25] Additionally, while Mn^{II} centers are adequately described by the spin magnetic moment (spin-only model), Co^{II} centers in octahedral or pseudo-octahedral environments are characterized by significant orbital moments, leading to spin–orbit coupling (SOC) effects that are expected to significantly affect more complex devices.

Our theoretical analysis, performed through a first-principles approach and a Heisenberg model Hamiltonian explains the marked experimental differences between the two compounds, opening the door to using *in silico* work to design complexes with targeted magnetic properties.

2 Methods

2.1 Theory

Theoretical calculations were performed in the Density Functional Theory (DFT) framework, using a pseudopotential description of the core electrons and atomic orbital basis set, as implemented in the SIESTA code.[26,27] We adopted the local density approximation (LDA)[28,29] for the exchange–correlation energy functional. A Hubbard correction for Mn and Co was included to account for the strong Coulomb interaction of localized d electrons. We use $U =$ 6 eV for Mn and $U = 4$ eV for Co, according to the literature.[21,30] To evaluate the role of spin–orbit coupling, which is relevant in Co, we also performed calculations including spin–orbit correction using the formalism of ref. 31, as implemented in SIESTA.[32] The current version of the SIESTA code does not allow to simultaneously include Hubbard and spin–orbit corrections, thus the two effects are treated separately.

The structure was relaxed with a tolerance on the forces on the atoms equal to 0.03 eV Å^{-1}. In the LDA+U calculations the finesse of the real-space grid (mesh-cutoff) was set to 400 Ry and the smearing of the electronic occupation (electronic temperature) to 100 K. In order to increase the accuracy in the convergence, SOC calculations where performed with 600 Ry mesh cutoff and 1 K electronic temperature. The structural relaxation has been refined with SOC, starting from the LDA+U equilibrium geometry. The exchange coupling parameters $J_{i,j}$ were obtained by considering the lowest energy spin configurations of the Mn and Co centers and solving a system of equations (Heisenberg model) in the DFT energies with four $J_{i,j}$ parameters. The geometry of the various spin configurations was kept fixed to the ground state one in order to exclusively account for the effect of the spin-flip on the total energy of the molecules.[33] Further, we exploited the model Heisenberg Hamiltonian $H = \sum_{i,j} \vec{S}_i \cdot J_{i,j} \cdot \vec{S}_j + \mu_B g \vec{S} \cdot \vec{B}$, where $\vec{S}_i$ is the spin vector of atom i and $J_{i,j}$ is the matrix of the exchange parameters, to fit experimental temperature and field-dependent magnetization data, as allowed by the implementation in the PHI code.[34] In the following we label $J_1 = J_{1,4} = J_{2,3}, J_2 = J_{1,3} = J_{2,4}, J_3 = J_{1,2}, J_4 = J_{3,4}$, with the M_i atoms numbered as indicated on Fig. 1.

2.2 Experiment

The complexes $[M_4L_2(OAc)_4]$ (M = Mn, Co, Zn, {M_4} for short), where H$_2$L = 2,6-bis-(1-(2-hydroxyphenyl)iminoethyl)pyridine,
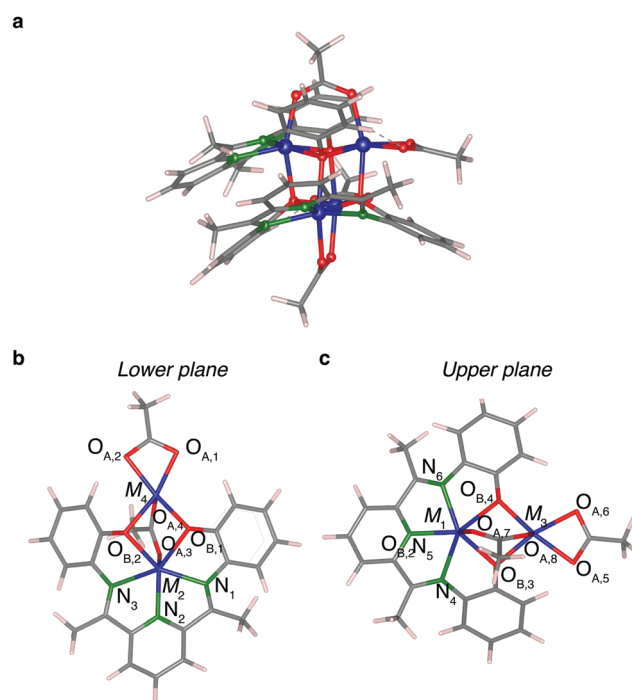

Fig. 1 Molecular structure of the {M_4} complex. (a) Side view. Blue: Mn, Co or Zn atoms; red: O; green: N; gray: C, white: H. (b) Top view of the lower half of the molecule. (c) Top view of the upper half of the molecule. Relaxed coordinates are available in ESI.†

This journal is © the Owner Societies 2022

Phys. Chem. Chem. Phys., 2022, **24**, 3780–3787 | **3781**

HOAc = acetic acid, and M = Mn^{II}, Co^{II} or Zn^{II}) were synthesized by one pot reaction of 2-aminophenol, diacetylpyridine and manganese, cobalt or zincacetate, as described by Kampert *et al.* for the manganese complex,[21] with some modifications for the cobalt and zinc analogues. Full details of the synthesis methods are given in the ESI.† The two new molecular complexes were characterized *via* single crystal diffraction conducted on a SuperNova (Agilent Technologies) diffractometer using Mo K radiation at 120 K. The crystals were mounted on a Hampton cryoloop with Paratone-N oil to prevent solvent loss. Thermogravimetric analysis was performed using a Mettler-Toledo TGA/SDTA 851e instrument with a heating rate of 10 K min^{-1}. Cyclic voltammograms were recorded in dry and deaerated acetonitrile solutions containing tetrabutylammonium perchlorate (0.1 M) as electrolyte and 3 mM of the analyte, using a SP-150 potentiostat (BioLogic Science Instruments) controlled by the EC-Lab software and a standard three-electrodes setup including a glassy carbon working electrode (diameter 3 mm), a platinum wire counter electrode and an Ag/AgNO$_3$ (0.1 M) reference electrode. Ferrocene was used as an internal standard. Magnetometry was performed on a Quantum Design MPMS-5XL SQUID magnetometer. The crystalline samples were crushed and placed under vacuum for 16 h before the complete removal of solvate molecules was checked by TGA. The resulting powders were compacted and immobilised into PTFE capsules. All data were corrected for the contribution of the sample holder (PTFE capsule). Measurements on {Zn$_4$} were used to determine the diamagnetic susceptibility of this complex $\chi_{dia}(Zn_4) = -5.3 \times 10^{-9}$ m^3 mol^{-1}. The diamagnetic contribution in {Co$_4$} and Mn$_4$ was then calculated from this value and Pascal's constants[35] for the Zn^{2+}, Co^{2+} and Mn^{2+} ions, yielding $\chi_{dia}(Co_4) = -5.1 \times 10^9$ m^3 mol^{-1} and $\chi_{dia}(Mn_4) = -5.2 \times 10^{-9}$ m^{-3} mol^{-1}, and subtracted from the experimental susceptibility data.

3 Theoretical and experimental analysis

3.1 Synthesis and redox properties

The {M$_4$} are stable towards oxidation in the solid state as well as in solution, despite the sensitivity of the {Co$_4$} precursors to oxidation by O$_2$ during synthesis. This observation is confirmed by the cyclic voltammetry of the complex (Fig. 2, purple dotted line), which displays two quasi-reversible ($\Delta E = 120$ mV) one-electron oxidation waves at 0.30 and 0.80 V *vs.* Fc$^+$/Fc which can be assigned as {Co$_4^{II}$} $\rightarrow$ {Co$_3^{II}$Co^{III}} $\rightarrow$ {Co$_2^{II}$Co$_2^{III}$}. As expected, the redox couples in the manganese complexes are shifted to lower potentials and show the large peak-to-peak characteristic of Mn^{II}(HS) $\rightarrow$ Mn^{III}(LS) processes (Fig. 2, yellow solid line). Finally, the zinc derivative shows irreversible ligand-centered oxidation processes above 0.5 V *vs.* Fc$^+$/Fc (Fig. 2, gray dashed line).

3.2 Molecular structure

The structure of the cobalt and zinc complexes was determined by single crystal X-ray diffraction to be analogue to that of the
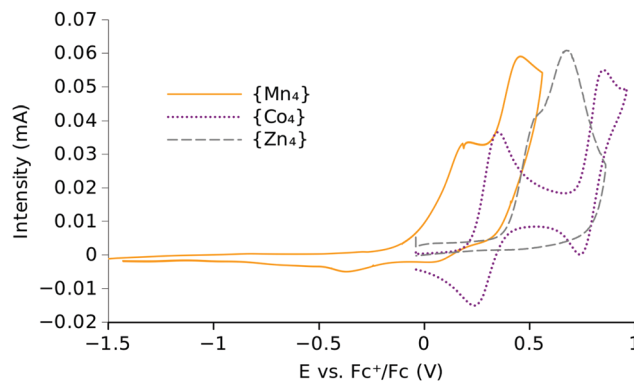

Fig. 2 Cyclic voltammograms of the {M$_4$} complexes (M = Mn, Co, Zn, concentration *ca.* 3 mM) in acetonitrile. Tetrabutylammonium perchlorate (0.1 M) is used as electrolyte and the scan rate is 50 mV s^{-1}.

previously published manganese complex:[21] the complexes consist of a cubic M$_4$O$_4$ core with two sets of two different ligand groups, for a total of 118 atoms (Fig. 1). The metallic core is a quasi-tetrahedron composed of two 7-coordinated ions (M$_1$, M$_2$) with pentagonal bipyramidal coordination and two 6-coordinated ions (M$_3$, M$_4$) with pseudo-octahedral symmetry.

The metal ions with the same coordination number are almost equivalent, as they overall face a quasi-identical chemical environment. The molecular cluster has an approximately C_2 symmetry and can be described as two identical structures on different planes that are rotated of 90° one respect to the other (Fig. 1), taking the rotation axis along z. Seven-coordinated M$_1$ and M$_2$ lie on different planes, each being connected in-plane to a pentadentate pyridine–diimine–diphenoxide type ligand (L^{2-}), completed by the oxygen of a bridging acetate and a κ^3 phenoxide oxygen from the other L^{2-} ligand. The coordination sphere of M$_3$, M$_4$ is a pseudo octahedron of six oxygen atoms provided by a bidentate acetate ligand, the other oxygen of the two bridging acetate and two phenoxide oxygen from the L^{2-} ligand (relaxed coordinates available in ESI†).

The inner cage of the three molecules is composed by four transition metal ions with different atomic valence configurations, 3d^5 for Mn(II), 3d^7 for Co(II) and 3d^{10} for zinc(II). The latter complex is therefore diamagnetic; it was used experimentally to determine the diamagnetic contribution to the susceptibility of the complexes and will not be discussed further. Both Mn(II) and Co(II) ions display high spin configurations, *i.e.* $S = 5/2$ for Mn and $S = 3/2$ for Co.

Despite the similarity between the structures of the manganese and cobalt complexes, experimental evidence and DFT calculations show small differences in bond lengths in the inner core. In agreement with the larger atomic radius of Mn with respect to Co, the {Mn$_4$} central cage is slightly larger than the {Co$_4$} one, due to larger M–O and M–N bond-lengths. Details of the structure are reported in Table 1.

3.3 Behavior in magnetic field

In order to quantify the strength of the magnetic interaction within the molecule and the response to an external magnetic

3782 | *Phys. Chem. Chem. Phys.*, 2022, **24**, 3780–3787

This journal is © the Owner Societies 2022

Table 1 Theoretical (DFT) and experimental (XRD) bond-lengths (Å) of the {Mn$_4$} and {Co$_4$} molecular complexes. XRD data was obtained at 208 K for {Mn$_4$}[21] and at 100 K for {Co$_4$}

d (Å)	M$_1$–M$_2$	M$_3$–M$_4$	M$_1$–M$_3$[a]	M$_2$–O$_{B,1}$[b]	M$_4$–O$_{A,2}$[b]
{Mn$_4$}					
DFT	3.35	3.45	3.64/3.65	2.20–2.30	2.15–2.22
XRD	3.62	3.47	3.50/3.55	2.27–2.31	2.21–2.22
{Co$_4$}					
DFT	3.26	3.21	3.42/3.44	2.15–2.21	2.07–2.11
XRD	3.39	3.19	3.15/3.16	2.17–2.29	2.11–2.19

[a] The two values correspond to the equivalent pairs of atoms. [b] Range given for all equivalent distances in the complex.

field we performed SQUID magnetometry experiments (Fig. 3). A singlet ground state is observed in both complexes, indicating the presence of antiferromagnetic coupling between the magnetic ions in the molecule. The molecular moment μ_{mol} as a function of magnetic field (H = 0–5 T) and temperature (T = 20–300 K) was fitted to a mean field model (Curie–Weiss law, eqn (1)), yielding Néel temperatures of T_N = 23 K for {Mn$_4$} and T_N = 12 K for {Co$_4$}:

$$\mu_{mol} = \frac{CH}{T - T_N} \qquad (1)$$

Those values, as well as the larger slope of the molecular moment at low field/low temperature observed for {Co$_4$} in comparison to {Mn$_4$}, suggests that the antiferromagnetic coupling between the metal atoms in {Co$_4$} is smaller than in {Mn$_4$}.

Notably, the behavior is reversed at high temperature with a larger magnetic moment for {Mn$_4$} than for {Co$_4$}, which is in agreement with the higher spin moment of the Mn centers.

The Curie constant C obtained for the {Mn$_4$} complex (3.0 × 10^{-3} μ_B K Oe^{-1}) is in good agreement with a spin-only model (3.1 × 10^{-3} μ_B K Oe^{-1} for g = 2 and S = 5/2). Such a model is not adequate for octahedral cobalt(II) complexes, with their $^4T_{1g}$ ground term, and effective orbital momentum L = 1.[36] Indeed, the Curie constant of {Co$_4$} (2.4 × 10^{-3} μ_B K Oe^{-1}) obtained from the Curie–Weiss fit deviates significantly from the one calculated by the spin-only model (1.3 × 10^{-3} μ_B K Oe^{-1}).

The measured magnetic susceptibility is reported in ESI,† together with the theoretical one obtained from spin dynamics
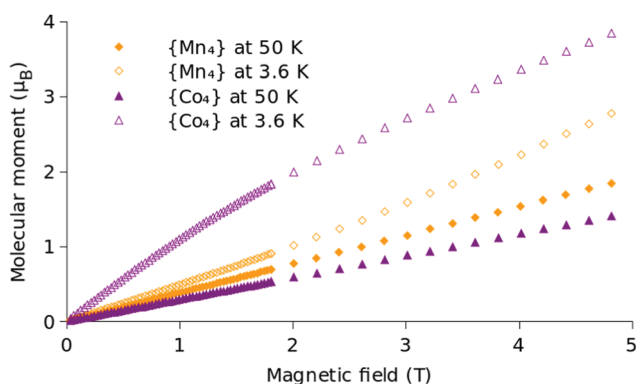
calculations. The agreement between theory and experiment is fairly good in the LDA+U approximation (see the discussion in Section 3.6).

3.4 Magnetic and electronic properties

In order to characterize the magnetic configuration of the inner cage and to ascertain the role of spin–orbit coupling in {Co$_4$} we performed DFT calculations which show that the ground state is characterized by an antiferromagnetic coupling between non-equivalent metal ions (M$_1$/M$_3$ and M$_2$/M$_4$), and a ferromagnetic one between the equivalent pairs (M$_1$/M$_2$ and M$_3$/M$_4$) giving rise to a up-up-down-down (uudd) configuration, referring to the relative alignment of the spins of the four metal ions. The magnetic moments of Co, Mn, N and O in the two molecular complexes, deduced from the Mulliken charge population, are reported in Table 2. Due to the chemical interaction with the ligands the magnetic moment of the metal atoms in the molecular complexes is reduced with respect to the isolated ions (∼4% in {Mn$_4$}, ∼10% {Co$_4$}). Accordingly, the induced magnetization of the ligands is smaller for {Mn$_4$} than for {Co$_4$}, as can be appreciated also through the small differences in the spatial distribution of the spin density ($\rho_{up} - \rho_{down}$ on the oxygen atoms, Fig. 4). In {Mn$_4$} the magnetic moment of O$_A$ and O$_B$ is negligible. In {Co$_4$} the bridging phenoxy oxygens have opposite magnetization: O$_{B2}$ and O$_{B3}$ are magnetized up while O$_{B1}$ and O$_{B4}$ are magnetized down. Out of the eight acetate oxygens O$_A$, only two (O$_{A+}$) display a small positive magnetic moment while the other six (O$_{A-}$) have a larger (in modulus) negative magnetic moment (mean value reported in Table 2). The average magnetization of the N atoms is comparable to the average contribution of O$_A$ but with opposite sign. As a consequence, despite the presence of local magnetic moments, the total spin

Table 2 Magnetic moment (μ_B) of the {Mn$_4$} and {Co$_4$} molecular complexes. Average values are reported for N (variance 0.004 μ_B), and O$_A$ atoms with positive (O$_{A+}$ = O$_{A_{3,7}}$) and negative (O$_{A-}$ = O$_{A_{1,2,4,5,6,8}}$) magnetic moment (variances in {Mn$_4$}/{Co$_4$} are 0.0/0.001 μ_B and 0.001/0.002 μ_B, respectively). Note the (anti)ferromagnetic coupling between (non-) equivalent metal ions: M$_1$ ∼ −M$_3$, M$_2$ ∼ −M$_4$, M$_1$ = M$_2$, M$_3$ = M$_4$

(μ_B)	M$_{1,2}$	M$_{3,4}$	N	O$_{A+}$	O$_{A-}$	O$_{B_{2,3}}$	O$_{B_{1,4}}$
{Mn$_4$}	4.82	−4.89	0.01	0.01	−0.01	0.00	0.00
{Co$_4$}	2.71	−2.73	0.05	0.03	−0.04	0.02	−0.02

Fig. 3 SQUID magnetometry data of {Mn$_4$} (orange) and {Co$_4$} (purple) at T = 3.6 K (open symbols) and T = 50 K (filled symbols).
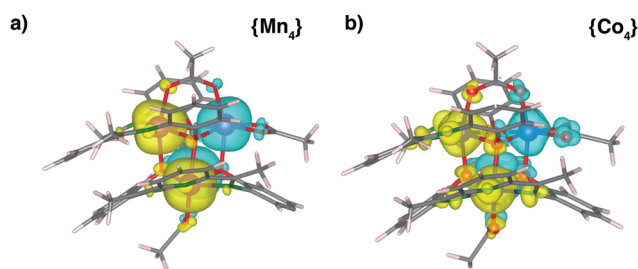

Fig. 4 Spin density on {Mn$_4$} and {Co$_4$}. Yellow (blue) isosurfaces correspond to positive (negative) values with a fixed value of 0.025. Spin density on the ligands is more pronounced in the {Co$_4$} case.

This journal is © the Owner Societies 2022

Phys. Chem. Chem. Phys., 2022, **24**, 3780–3787 | **3783**

of both molecules is $S_{TOT} = 0$ confirming their antiferromagnetic character. Nevertheless, the major spread of the magnetic moment observed in {Co$_4$} is an indication of a possible large magnetic interaction of this molecule with other systems when the complex is used for functionalization.

In Fig. 5 the DOS of the two molecules projected on different atoms of the complex (PDOS), is reported. The PDOS of Mn ions is characterized by the prevalence a single spin population, due to the almost complete filling of the spin-up 3d electrons. In Co, instead, majority and minority spins are present, according to the more-than-half filling of the 3d orbitals. The oxygen atoms display a different PDOS depending on the group they are attached to. In particular the states of the bridging oxygen atoms O$_B$ partially overlap with the states of the magnetic ions, with larger extent for the seven-coordinated ones (M$_{1,2}$) in the majority-spin component and with the six-coordinated ones (M$_{3,4}$) in the minority spin component. This overlap, which appears to be slightly more intense in {Mn$_4$}, is responsible for the coupling between magnetic ions *via* superexchange interaction mechanism.[37]

For both complexes, the O$_A$ atoms are characterized by majority spin states in the $[-3, -1]$ eV energy range and minority states centered around -2.5 eV, with a moderate overlap with the metal atoms in both cases. We can therefore conclude that they contribute to the magnetic coupling between metal centers with a similar strength.
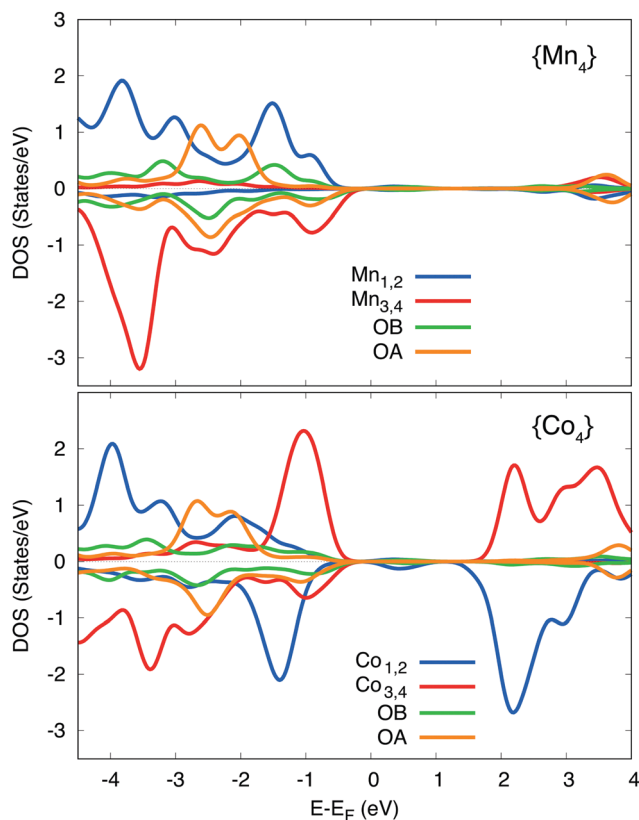
Table 3 Net atomic charges of the atomic species in the {Mn$_4$} and {Co$_4$} molecular complexes (in units of electron charge e). Positive (negative) values indicate donor (acceptor) behavior. Average values are reported for the equivalent centers

Δq (e)	M$_{1,2}$	M$_{3,4}$	N	O$_A$	O$_B$
{Mn$_4$}	+1.10	+1.32	+0.29	−0.39	−0.60
{Co$_4$}	+1.49	+1.63	+0.21	−0.44	−0.68

The hybridization with states of the ligands is also responsible for the charge transfer from the magnetic ions to the nearby atoms. In the molecular complexes, Mn and Co atoms display a number of electrons smaller than the valence of the isolated atom, as reported in Table 3 in term of the net atomic charge, *i.e.* they donate electron charge. This reduction of charge is larger for the two metal ions bound to the pyridine–diimine group (M$_{1,2}$) with respect to the 6-coordinated magnetic atoms in the same molecule (M$_{3,4}$). Moreover, the percentage of lost charge is larger in {Mn$_4$} ($\sim 25\%$) than in {Co$_4$} ($\sim 22\%$), according to the larger hybridization with the surrounding coordination groups. The oxygen atoms act as electron acceptors in both molecules. The maximum charge transfer is toward the bridging oxygens that acquire 0.60 and 0.68 electrons (mean values) in {Mn$_4$} and {Co$_4$}, respectively. For O$_A$ atoms the absolute values of the acquired charge ($\sim 0.4e$) are similar in the two complexes. N atoms participate to charge transfer towards the ligands by donating electrons, with a slightly larger fraction in {Mn$_4$} ($\sim 0.29e$) than in {Co$_4$} ($\sim 0.21e$). On the basis of the results reported by Kampert *et al.*[21] the charge withdrawn from the [M$_4$O$_4$] core (by the ligands) is inversely proportional to the strength of the magnetic interaction within the complex. For both complexes, the analysis of Mulliken charges predicts that the [M$_4$O$_4$] core acts as a donor, with 2.45 and 3.43 electrons donated in the Mn and Co case, respectively. Therefore, we expect that a stronger antiferromagnetic coupling in {Mn$_4$} than in {Co$_4$}, supporting the experimental findings.

3.5 Role of spin orbit coupling

In the previous paragraphs we have analyzed the results obtained with the LDA+U approximation, necessary to account for the electronic correlation of localized 3d orbitals, but limited in the SIESTA code to a collinear-spin description of magnetism. This approximation is valid for the Mn(ɪɪ) ions, as the high-spin d^5 electronic configuration does not have a net orbital momentum. In Co(ɪɪ) centers, instead, the d^7 configuration leads to an orbital momentum $L = 3$ for an isolated ion. While the orbital momentum is quenched in low symmetry environments, including pentagonal bipyramidal, it is not in a perfect octahedron, where $L = 1$. As two of the metal centers in {Co$_4$} display a pseudo-octahedral geometry, SOC is expected to have a significant effect on the magnetic properties of this complex.

In order to investigate the role of SOC in the complexes, we have performed DFT calculations including SOC for both molecules at $U = 0$ using the fully relativistic pseudopotential formalism[31] implemented in SIESTA.[32] The magnetization

Fig. 5 Density of states projected on the magnetic ions and different oxygen atoms (O$_A$ and O$_B$) in the two molecular complexes. The average PDOS per atom type is reported.

direction has been set along the z axis for {Mn$_4$}. Indeed we verified that for this molecule the magnetic anisotropy related to spinflip along five independent directions is at most ~ 100 μeV per molecule. For {Co$_4$}, which is expected to display strong spin–orbit effects, we have explored 30 different direction of the magnetization. The easy axis for {Co$_4$} is rotated with respect to the z direction with a polar angle 150° and azimuthal angle 45°. The maximum magnetic anisotropy for spinflip amounts to 12 meV per molecule. The results reported below are relative to {Co$_4$} with the spin along the easy axis.

In Tables 4 and 5 the computed S, L, and their sum (J) are reported for both molecular complexes. In both cases, the atomic spin is slightly reduced with respect to the LDA+U calculation. The four metal ions in {Co$_4$} display an orbital moment which is smaller than the value expected for the isolated ion, but significantly larger than the manganese analogue. The quenching is stronger for the two ions in the pentagonal bipyramidal coordination, for which $\sqrt{\langle L^2 \rangle} \sim 0.15$. For the 6-coordinated pseudo-octahedral Co ions L is not negligible (~ 0.4) and contributes to an overall value of $\sqrt{\langle J^2 \rangle} \sim 3$.

Table 4 Spin (S), orbital moment (L) and their composition (J) for the four magnetic atoms of the {Mn$_4$} core. The data are reported in units of μ_B

	Mn$_1$	Mn$_2$	Mn$_3$	Mn$_4$
$\sqrt{\langle S^2 \rangle}$	4.33	4.37	4.34	4.34
S_x	1.43	−1.35	0.17	0.37
S_y	1.097	−0.59	−0.20	0.058
S_z	3.94	4.11	−4.33	−4.32
$\sqrt{\langle L^2 \rangle}$	0.052	0.057	0.058	0.058
L_x	0.013	−0.015	−0.007	−0.003
L_y	0.006	−0.008	0.004	0.01
L_z	0.05	−0.054	−0.057	−0.057
$\sqrt{\langle J^2 \rangle}$	4.38	4.40	4.39	4.40

Table 5 Spin S, orbital moment L and their composition (J) for the four magnetic atoms of the {Co$_4$} core. The data are reported in units of μ_B

	Co$_1$	Co$_2$	Co$_3$	Co$_4$
$\sqrt{\langle S^2 \rangle}$	2.56	2.56	−2.57	−2.58
S_x	−0.19	1.92	−1.92	0.975
S_y	1.355	1.6	−1.62	−0.72
S_z	−2.61	−0.56	−0.52	2.29
$\sqrt{\langle L^2 \rangle}$	0.15	0.14	0.46	0.35
L_x	−0.004	0.121	−0.33	0.057
L_y	0.051	0.065	−0.33	0.06
L_z	−0.14	−0.033	−0.033	0.33
$\sqrt{\langle J^2 \rangle}$	2.71	2.71	3.03	2.92

3.6 Exchange coupling

In order to ascertain the strength of the (anti)ferromagnetic coupling in the two complexes we computed the exchange coupling parameters (J_i) from first-principles total energies by considering the five lowest-energy spin configurations of the molecules (uudd, udud, uddu, uddd, uuuu) as explained in Section 2.1. The calculated exchange parameters, obtained in the LDA+U approximation, are reported in Table 6, where positive and negative values correspond to ferromagnetic (FM) or antiferromagnetic (AFM) coupling.

The calculated J_i are of the same order of magnitude of those extracted from experimental susceptibility (see ESI†), and are in fair agreement with those reported in ref. 21 for a three-J model. Both J_1 and J_2 are negative, confirming the antiferromagnetic coupling between not equivalent atoms. One of the other two parameters describing the coupling between equivalent atoms (J_3 or J_4) is positive (FM), in agreement with the data extracted from the experiments. The overall exchange interaction, estimated as the average of the J_s (-3.7 meV for {Co$_4$} and -1.4 for {Mn$_4$}), is AFM for both molecular complexes.

The strongest J_i (J_1 in {Co$_4$}, J_2 in {Mn$_4$}) corresponds to the interaction between the two pairs of not-equivalent ions and it is related to the energy difference between the AFM ground state and the high spin FM state ($S = 12$ for {Co$_4$} and $S = 20$ for {Mn$_4$}) which is larger for {Co$_4$}. The FM interaction between equivalent ions (intra-pair) is, instead, smaller for {Co$_4$}. The latter governs the transition to low-spin FM states (for example uddd) which influences the behavior of the magnetization at low fields and low temperatures, hence explaining the observed switching with temperature of the magnetization curves $M(B)$ of the two molecules (Fig. 3). To further explore this behavior, we have exploited a model Heisenberg Hamiltonian with J parameters and g-factor fitted from the experimental low-field susceptibility (ESI†) and used them to calculate $M(B)$ at two different temperatures. We find that the observed (Fig. 3) switch of $M(B)$ with temperature is an effect of the more marked AFM character of {Mn$_4$} giving rise to a positive curvature of $M(B)$ at low field/low T. At high field/high T, instead, the most relevant factor is the larger saturation value of the magnetization in {Mn$_4$} compared to {Co$_4$}. By increasing the range of the magnetic field beyond the experimental one, a crossing of the two theoretical curves is observed due to the combination of these two aspects (ESI†).

The inclusion of SOC in the calculation leads to J_s with a sign that reflects the uudd magnetic order of the ground state, *i.e.* AFM (FM) coupling between M1/M4 and M2/M3 non-equivalent (M1/M2 and M3/M4 equivalent) ions (see Table S2 in ESI†). Nevertheless, the exchange parameters obtained with

Table 6 Exchange coupling parameters (J_i, meV) of {Mn$_4$} and {Co$_4$} molecular complexes extracted from DFT calculations with LDA+U. S is normalized to 1

LDA+U (meV)	J_1	J_2	J_3	J_4
{Mn$_4$}	−0.2	−0.9	−0.2	0.9
{Co$_4$}	−1.8	−0.19	0.8	−0.6

This journal is © the Owner Societies 2022

Phys. Chem. Chem. Phys., 2022, **24**, 3780–3787 | **3785**

SOC are too large compared to those extracted from the experiments,[21] suggesting that the electronic correlation can not be neglected for a reliable estimate of the strength of the magnetic interactions. A complete description of the magnetic properties of the clusters requires treating spin–orbit coupling and Hubbard-U correction on the same footing. However, the usual formulation of the Hamiltonian for exchange interaction only depends on the spin quantum number. This is accurate when the orbital moment are negligible with respect to the spin moment. We verified this is the case (Table 4) and use the LDA+U approximation to predict the exchange coupling parameters.

For a deeper insight of the exchange interaction, we have computed the exchange parameters also with the Liechtenstein–Katsnelson–Antropov–Gubanov (LKAG) formula[38] implemented in the TB2J package,[39] which treats the local spin rotation of the numerical atomic orbitals for the magnetic atoms as a perturbation.

The J_i, evaluated with this approach present the same overall trend as those computed from total energies (Table 6), for both LDA+U and SOC case, and are reported in the ESI† (Table S3).

The different predictions of the various approximations (LDA+U or SOC) are a consequence of the complexity of the magnetic potential energy landscape of these molecular complexes. A small perturbation (geometry, electron correlation, spin alignment) can drive the results out of equilibrium and towards a different local minimum. Despite these difficulties, all the computed J_i parameters predict the experimentally observed uudd ground state, regardless of the approach (total energies or perturbative) and inclusion of correlations or SOC. This has been verified by feeding the computed J_i in the Heisenberg Hamiltonian and computing the various spin configurations (Fig. S3, ESI†).

Finally, we used all the computed J_i parameters as input for spin dynamics simulations[40–42] to predict the magnetic susceptibility, finding a good agreement with experiment in the LDA+U case (ESI†). The results obtained without U correction are, instead, in striking contradiction with experiments, confirming the importance of taking into account electron correlation in the transition metal sites.

4 Conclusions

Through a joint experimental and theoretical analysis we have characterized the properties of two coordination complexes, {Mn$_4$} and {Co$_4$}, that display the same chemical structure but different inner magnetic core formed by Mn and Co atoms, respectively. The theoretical analysis was performed under different approximations (LDA+U, SOC) and methods (first-principles, model Hamiltonians, perturbation theory).

The experimental data and the theoretical calculations show that by changing the magnetic core, the robustness of the AFM configuration in an external magnetic field is changed, being stronger in {Mn$_4$} than in {Co$_4$}. The reason for this behavior can be found in the different interaction of the magnetic atoms with the surrounding ligands, which determines a different

strength of the magnetic interaction within the molecule. This result confirms the possibility to tune the magnetic properties of the molecule through the chemical synthesis by acting on the magnetic inner core. Nevertheless, a general rule explaining the relationship between the choice of the magnetic atoms and the magnetic coupling in the molecule can not be established because the ligands, which are molecule-specific, also play a role. We also verified that the different magnetic properties of the two chemical species lead to a different spatial extension of the magnetic moment and electronic charge density on the ligands, which could influences the interaction with foreign systems and affects the efficiency of the two compounds when employed for magnetic functionalization.

We find and explain an unusual switch with temperature of the dependence of the magnetic moment from the applied magnetic field $M(B)$ for the two molecules. We relate it to two competing effects: the stronger AFM coupling in {Mn$_4$} and the large value of magnetization in {Mn$_4$} which dominate at low and high temperature, respectively.

The calculations clarify the role of spin–orbit effects: negligible in {Mn$_4$} and relevant in {Co$_4$}, showing that SOC has to be considered for a reliable theoretical description of the magnetic moments of the latter. In perspective of future exploitation of these compounds in spintronics the SOC effects found in {Co$_4$} should be taken into account as possible source of spin decoherence.

Our study of the exchange coupling parameters and spin dynamics demonstrate that it is necessary to explicitly include electron correlations (for instance, *via* a Hubbard U parameter) to properly recover these properties. The complete description of the molecular complexes can only be performed in a framework in which electronic correlation and SOC are treated on the same footing.

Conflicts of interest

There are no conflicts to declare.

Acknowledgements

3786 | *Phys. Chem. Chem. Phys.*, 2022, **24**, 3780–3787

This journal is © the Owner Societies 2022

Notes and references

1 M. Ganzhorn and W. Wernsdorfer, *Molecular Magnets*, Springer, Berlin, Heidelberg, 2014.
2 E. Coronado, *Nat. Rev. Mater.*, 2020, **5**, 87–104.
3 M. Gobbi, M. A. Novak and E. Del Barco, *J. Appl. Phys.*, 2019, **125**, 240401.
4 D. Maniaki, E. Pilichos and S. P. Perlepes, *Front. Chem.*, 2018, **6**, 461.
5 L. Bogani and W. Wernsdorfer, *Nat. Mater.*, 2008, **7**, 179–186.
6 Z. Zanolli, R. Leghrib, A. Felten, J.-J. Pireaux, E. Llobet and J.-C. Charlier, *ACS Nano*, 2011, **5**, 4592–4599.
7 Z. Zanolli and J.-C. Charlier, *ACS Nano*, 2012, **6**, 10786–10791.
8 H. Oshio and M. Nakano, *Chem. – Eur. J.*, 2005, **11**, 5178–5185.
9 S. Brooker and J. A. Kitchen, *Dalton Trans.*, 2009, 7331–7340.
10 K. S. Pedersen, J. Bendix and R. Clerac, *Chem. Commun.*, 2014, **50**, 4396–4415.
11 T. Jungwirth, X. Marti and P. Wadley, *Nat. Nanotechnol.*, 2016, **11**, 231–241.
12 M. Bragato, S. Achilli, F. Cargnoni, D. Ceresoli, R. Martinazzo, R. Soave and M. I. Trioni, *Materials*, 2018, **11**, 2030.
13 N. Makoto, H. Satoru, K. Hiroaki, Y. Yuki, M. Yukitoshi and S. Hitoshi, *Nat. Commun.*, 2019, **10**, 4305.
14 X.-X. Fu, F. Wei, Y. Niu and C.-K. Wang, *Phys. E*, 2021, **131**, 114737.
15 V. Baltz, A. Manchon, M. Tsoi, T. Moriyama, T. Ono and Y. Tserkovnyak, *Rev. Mod. Phys.*, 2018, **90**, 015005.
16 R. Frielinghaus, C. Besson, L. Houben, A.-K. Saelhoff, C. M. Schneidera and C. Meyer, *RCS Adv.*, 2015, **5**, 84119.
17 C. Besson, P. Stegmann, M. Schnee, Z. Zanolli, S. Achilli, N. Wittemeier, A. Vierck, R. Frielinghaus, P. Kögerler, J. Maultzsch, P. Ordejón, C. M. Schneider, A. Hucht, J. König and C. Meyer, 2021, arXiv:2107.07723.
18 A. Ardavan, O. Rival, J. J. L. Morton, S. J. Blundell, A. M. Tyryshkin, G. A. Timco and R. E. P. Winpenny, *Phys. Rev. Lett.*, 2007, **98**, 057201.
19 Y. Yu, C. Li, B. Yin, J.-L. Li, Y.-H. Huang, Z.-Y. Wen and Z.-Y. Jiang, *J. Chem. Phys.*, 2013, **139**, 054305.
20 B. Yin, J. Li, H. Bai, Z. Wen, Z. Jiang and Y. Huang, *Phys. Chem. Chem. Phys.*, 2012, **14**, 1121–1130.
21 E. Kampert, F. F. B. J. Janssen, D. W. Boukhvalov, J. C. Russcher, J. M. M. Smits, R. de Gelder, B. de Bruin, P. C. M. Christianen, U. Zeitler, M. I. Katsnelson, J. C. Maan and A. E. Rowan, *Inorg. Chem.*, 2009, **48**, 11903–11908.
22 M.-L. Tong, S.-L. Zheng, J.-X. Shi, Y.-X. Tong, H. K. Lee and X.-M. Chen, *J. Chem. Soc., Dalton Trans.*, 2002, 1727–1734.
23 G. S. Papaefstathiou, A. Escuer, F. A. Mautner, C. Raptopoulou, A. Terzis, S. P. Perlepes and R. Vicente, *Eur. J. Inorg. Chem.*, 2005, 879–893.
24 T. A. Hudson, K. J. Berry, B. Moubaraki, K. S. Murray and R. Robson, *Inorg. Chem.*, 2006, **45**, 3549–3556.
25 C.-B. Tian, H.-B. Zhang, Y. Peng, Y.-E. Xie, P. Lin, Z.-H. Li and S.-W. Du, *Eur. J. Inorg. Chem.*, 2012, 4029–4035.
26 J. M. Soler, E. Artacho, J. D. Gale, A. Garca, J. Junquera, P. Ordejón and D. Sánchez-Portal, *J. Phys.: Condens. Matter*, 2002, **14**, 2745.
27 A. García, N. Papior, A. Akhtar, E. Artacho, V. Blum, E. Bosoni, P. Brandimarte, M. Brandbyge, J. I. Cerdá1, F. Corsetti, R. Cuadrado, V. Dikan, J. Ferrer, J. Gale, P. García-Fernández, V. Garcá-Suárez, S. García, G. Huhs, S. Illera, R. Korytár, P. Koval, I. Lebedeva, L. Lin, P. López-Tarifa, S. G. Mayo, S. Mohr, P. Ordejón, A. Postnikov, Y. Pouillon, M. Pruneda, R. Robles, D. Sánchez-Portal, J. M. Soler, R. Ullah, V. Wen-zhe Yu and J. Junquera, *J. Chem. Phys.*, 2020, **152**, 204108.
28 W. Kohn and L. J. Sham, *Phys. Rev. B*, 1965, **140**, A1133.
29 D. M. Ceperley and B. J. Alder, *Phys. Rev. Lett.*, 1980, **45**, 566.
30 A. M. Ritzmann, M. Pavone, A. B. Muñoz García, J. A. Keith and E. A. Carter, *J. Mater. Chem. A*, 2014, **2**, 8060–8074.
31 R. Cuadrado and J. I. Cerdá, *J. Phys. Condens. Matter*, 2012, **24**, 086005.
32 R. Cuadrado, R. Robles, A. García, M. Pruneda, P. Ordejón, J. Ferrer and J. I. Cerdá, *Phys. Rev. B*, 2021, **104**, 195104.
33 Z. Zanolli, C. Niu, G. Bihlmayer, Y. Mokrousov, P. Mavropoulos, M. J. Verstraete and S. Blügel, *Phys. Rev. B*, 2018, **98**, 155404.
34 N. F. Chilton, R. P. Anderson, L. D. Turner, A. Soncini and K. S. Murray, *Phys. Rev. Lett.*, 2013, **34**, 1164.
35 G. A. Bain and J. F. B. Berry, *J. Chem. Ed.*, 2008, **85**, 532–536.
36 F. Lloret, M. Julve, J. Cano, R. Ruiz-García and E. Pardo, *Inorg. Chim. Acta*, 2008, **361**, 3432–3445.
37 J.-P. Launay and M. Verdaguer, *Electrons in molecules*, Oxford University Press, 2014.
38 A. I. Liechtenstein, M. I. Katsnelson, V. P. Antropov and V. A. Gubanov, *J. Magn. Magn. Mater.*, 1987, **67**, 65–74.
39 X. He, N. Helbig, M. J. Verstraete and E. Bousquet, *Comput. Phys. Commun.*, 2021, **264**, 107938.
40 L. Landau and E. Lifshitz, *Perspectives in Theoretical Physics*, Elsevier, 1992, pp. 51–65.
41 T. L. Gilbert, *IEEE Trans. Magn.*, 2004, **40**, 3443–3449.
42 X. Gonze, B. Amadon, G. Antonius, F. Arnardi, L. Baguet, J.-M. Beuken, J. Bieder, F. Bottin, J. Bouchet and E. Bousquet, *et al.*, *Comput. Phys. Commun.*, 2020, **248**, 107042.

This journal is © the Owner Societies 2022

Phys. Chem. Chem. Phys., 2022, **24**, 3780–3787 | 3787